Effect of Surface Films on Wave Amplitude and Dispersion of a Film by Wave Breaking

T. Schlicke[1], J. M. Buick[2], A. D. Arnott[1], C. A. Greated[1] and N. H. Thomas[2]

[1] Department of Physics and Astronomy, JCMB, The University of Edinburgh, Mayfield Road Edinburgh EH9 3JZ, UK
[2] CEAC, Aston University, Birmingham, B4 7ET, UK

1 Introduction

The presence of a surface film has been shown to alter the motion of surface capillary gravity waves [1, 2]. The interaction between waves and a surface film depends on factors such as: chemical composition of the film, its thickness, wave parameters coupled with bed slope and wind. A film acts to damp small scale waves, preventing their build up into larger waves which may break. Ironically, the breaking process is the primary mechanism for rapid dispersal of the film itself, therefore an understanding of the interaction is important. The work of [1, 2] is extended using 2 approaches:
a) The mixing of a surface film after a breaking event, using the technique of Laser Induced Fluorescence (LIF) and
b) A study of how the effect of a film affects steep gravity waves with parasitic capillary waves riding on the leading face.

The work is ongoing, in this paper some of the effects of different breaking wave amplitudes on the mixing process are presented, along with preliminary work on how the surface film damps waves and affects the energy transfer between different length scales in the waves.

2 Clean and Contaminated Surfaces

The dynamics of ocean waves can be influenced significantly by the presence of a surface film of contaminant, even if the thickness of the film is of the order of its molecular thickness. In fact, in a wave tank experiment, it can be necessary to follow a lengthy cleaning procedure [3, 4] to ensure that the surface is clean. In numerical wave simulations, a clean surface is generally used, despite evidence of surface films in the ocean. Two major differences between a clean and contaminated surface are the tangential stress at the wave surface and the dissipation rate. On a clean surface the tangential stress is zero and the dissipation varies as $1/Re$ [5], where Re is the Reynolds number, while on a contaminated surface the tangential stress can be non-zero and the dissipation varies as $\sqrt{1/Re}$ [6].

3 LIF Apparatus

The breaking wave is generated by a computer-controlled paddle in a flume $9.7m$ long by $0.4m$ wide, with a still water depth of $0.75m$. The paddle generates waves of between $0.5Hz$ and $1.5Hz$ in frequency. These are focussed at a specific distance downstream to produce a breaking wave.

The tank is illuminated by a thin, pseudo lightsheet, created by directing an Argon-ion laser beam onto a rotating, octagonal mirror (figure 1 top). Two Pulnix TM9701 cameras with $28mm$ Nikkon lenses are positioned $3m$ from the tank at identical heights and approximately $1m$ apart such that their fields of view overlap slightly. This allows the images from each camera to be combined into a single, 'widescreen' picture of the motion. The cameras are triggered at 20 frames per second by pulses emitted from a signal generator, the sequence starting from a gated signal

from the the computer controlling the wave paddle. The image data is captured by a Coreco Viper Quad framegrabber and stored in RAM. Over 2000 images can be stored in a single experiment.

The surface film consists of a solution of $1g$ of Rhodamine B per litre of methanol. Rhodamine B is highly fluorescent, producing bright orange light when illuminated by green laser light. A narrow band-pass filter is placed in front of each camera lens so that only the orange light emitted by the Rhodamine B falls onto the CCD arrays. In this way, Rhodamine concentrations as low 0.0005% can be detected. Five millilitres of this solution is carefully added to a porous float. Additional water is slowly poured onto this float, expelling the rhodamine solution and spreading it over the flume surface. Once the experiment is over, these images are corrected for variation

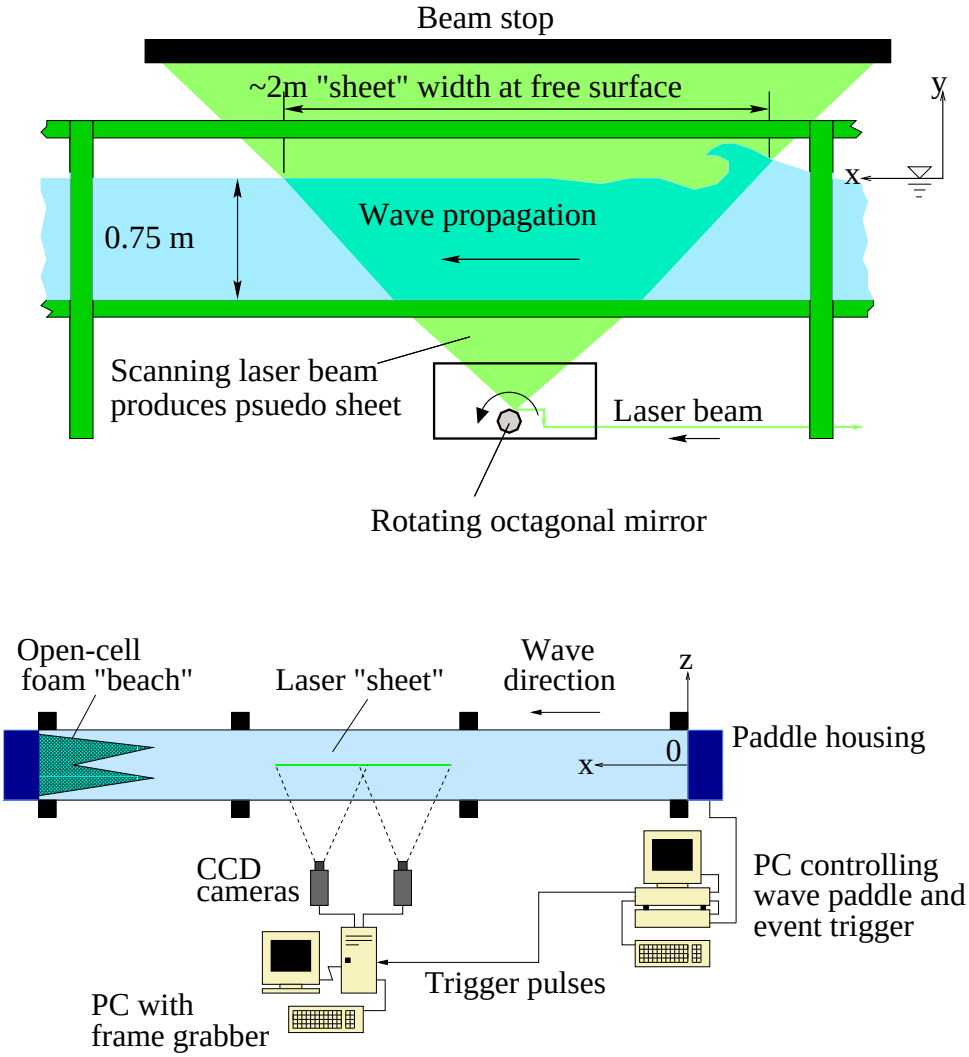

Figure 1: LIF illumination (top) and plan of Apparatus (bottom)

in the lightsheet intensity and calibrated such that their grey level values correspond to specific concentrations of rhodamine. The images are then combined by software written by the authors.

4 LIF Analysis

Three such images are shown in figure 2. They have been false coloured: purple corresponds to maximum concentration of ($\geq 0.02\%$), red to minimum concentration (0.0005%). Negligible dispersion of the film occurs before the surface has broken (figure 2a). Then the tip of a breaking

wave drives some of the contaminant downwards, creating an initial mixing region of rhodamine. The splash-up of the breaking event then produces a second, larger mixing patch, downstream of the first. Various parameters of the film distribution have been calculated in order to quantify the

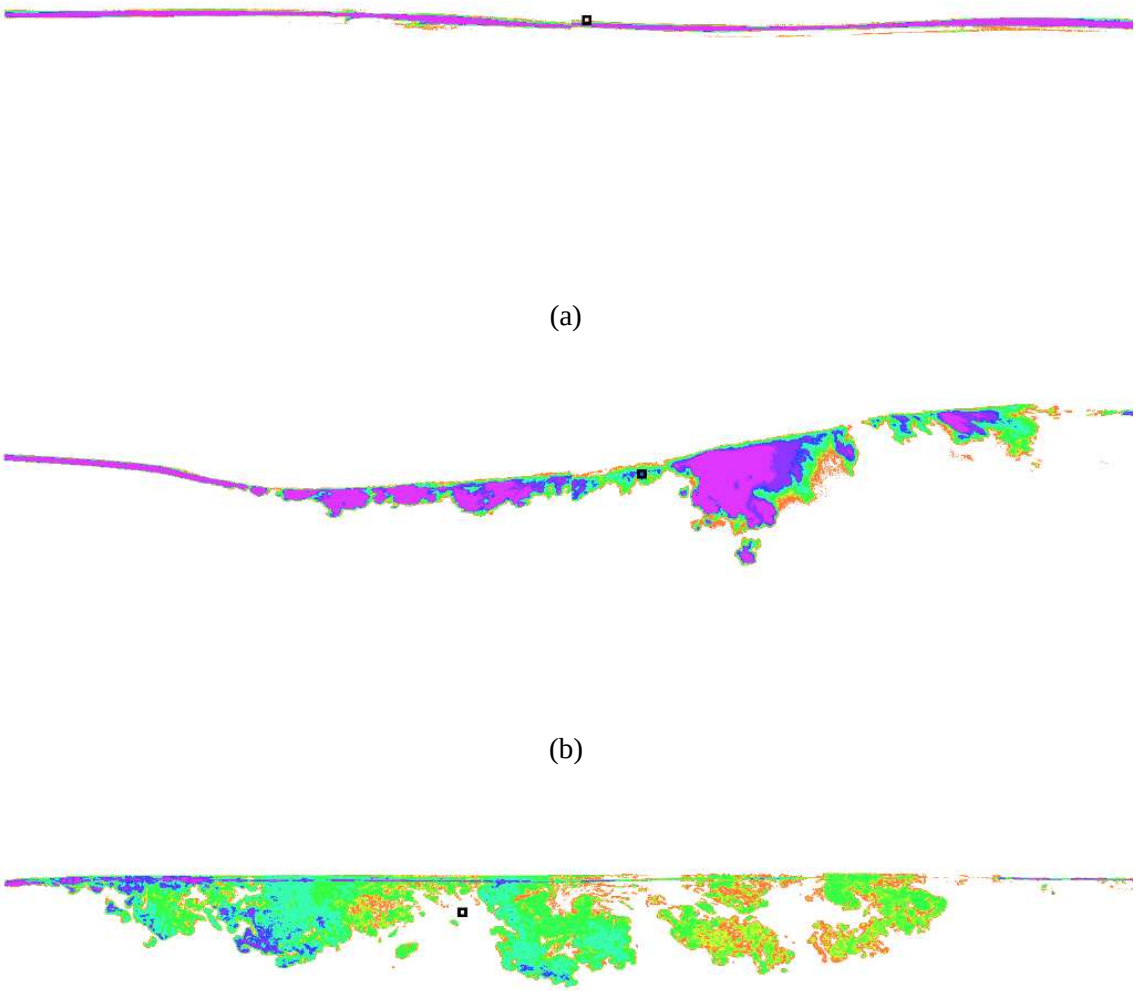

Figure 2: Surface Film prior to breaking (a), 1s (b) and 10s (c) after breaking

dispersion. Gross properties, such as maximum depth reached and total area covered, have been evaluated as functions of both concentration and time. These parameters were also investigated by Rapp and Melville [7], allowing a direct comparison of results. The position of the film's centre of mass has been followed, which reveals the net motion of the film. The centre of mass of each image in figure 2 is indicated by a small square. The diffusion of the film, or rate of expansion, can also be calculated using

$$\sigma^2 = 2Dt \tag{1}$$

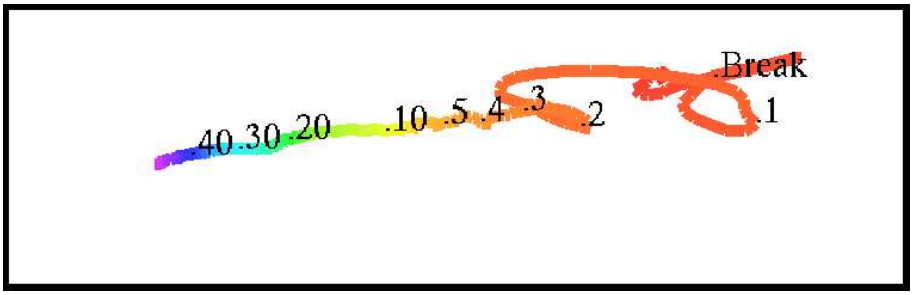

Figure 3: Motion of Film's Centre of Mass

where σ^2 is the variance of the concentration distribution, D is the diffusion coefficient and t is time.

The motion of the water prior to breaking is largely two dimensional in the $x-y$ plane; there is negligible movement in the z direction, perpendicular to the lightsheet. At this time, the film itself is effectively two dimensional in the $x-z$ plane, since the thickness of the film is several orders of magnitude smaller than either its length or breadth. After breaking, however, the film begins to disperse in the y direction, the 2-dimensional motion of the water evolving into 3-dimensions [8]. The out-of-plane motion of the water is responsible for the isolated patches of film which appear in the dispersion images. The decay of the turbulence towards higher wavenumbers has the effect of introducing increased detail at smaller scales to the outline of the film.

The film's transition from 2d to 3d can be described mathematically in terms of an increasing box-counting, or *fractal*, dimension F_D. The fractal dimension of an object is defined by

$$D_F = \lim_{r \to 0} \frac{\log N}{\log \frac{1}{r}} \tag{2}$$

where N is the number of squares of side r needed to cover the object.

The parameters mentioned so far are all scalar quantities. It is also possible, however, to obtain a vector map of the local velocities present in the film at a particular time. This is done by subdividing two images, taken a short time apart, and correlating the subsections, as in Particle Image Velocimetry [1].

5 Results

In this section, some of the effects of wave amplitude on dispersion characteristics are described. Wave amplitude is expressed as a non-dimensional number, ak_c, where a is the amplitude in metres and k_c is the central wavenumber of the wave components which combine to produce the breaking event. In the wave flume used in these experiments, it was found that if ak_c is less than approximately 0.28, breaking will not occur. Results from experiments involving three different wave amplitudes are presented. These amplitudes are $ak_c = 0.3$, corresponding to a spilling breaker, $ak_c = 0.326$, a weakly-plunging breaker and $ak_c = 0.352$, a strongly plunging-breaker.

The motion of the film's centre of mass as a function of time for the weak-plunging breaker is shown in figure 3. The position of the centre of mass at breaking is signified by 'break'; the numbers signify the time in seconds since breaking. For the first 3 seconds, the centre of mass position is dominated by the motion of the passing crests and troughs. After this time, however, the centre of mass moves at a fairly steady speed of approximately 2% the pre-breaking wave velocity in a uniform direction. This angle of descent was found to increase with ak_c. Figure 4 contains graphs of fractal dimension and diffusion against time for each of the three values of ak_c.

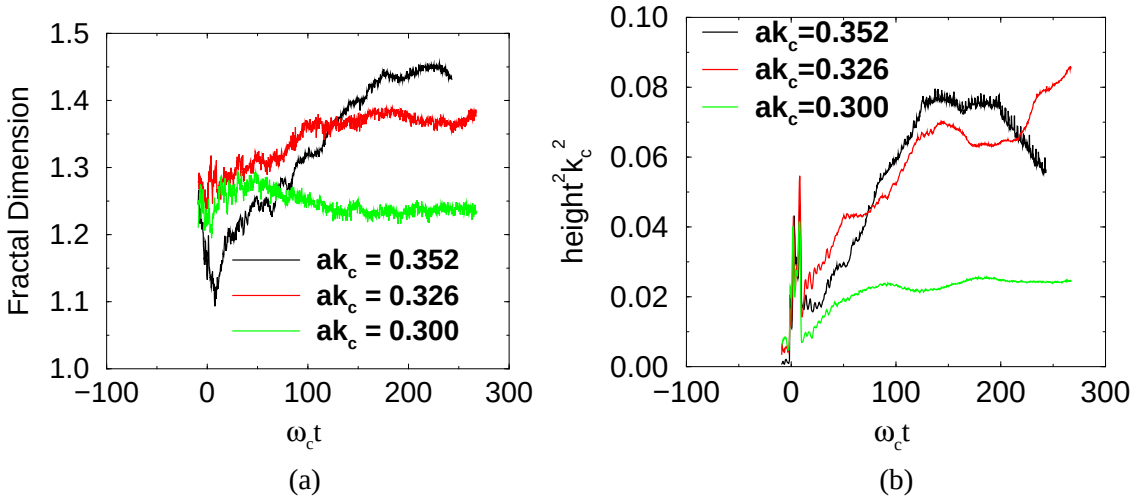

Figure 4: Graph of Fractal Dimension vs time (a) and Diffusion vs time (b)

In practice, it proved difficult to apply the rhodamine film without it forming a few faint tails into the bulk of the water. The fractal dimension of the film's outline prior to breaking is thus greater than one; approximately 1.25. All three curves appear to tend towards steady values with time. Both the time taken to reach this value, and the value itself, increase with ak_c.

The diffusion coefficients are the gradients of the curves in figure 4(b). Once again, the diffusion coefficient immediately after breaking is larger for higher values of ak_c. The negative diffusion coefficient for the strong plunging breaker is due to film moving outwith the field of view of the camera combination.

6 Parasitic Capillary Waves

6.1 Background

According to linear wave theory, applicable to small amplitude waves in deep water, the speed of propagation of a wave, c, is given by [9]

$$c = \frac{\omega}{k} = \left(\frac{g + \rho^{-1} T k^2}{k} \right)^{1/2}, \tag{3}$$

where g is the acceleration due to gravity, T is the surface tension, ω is the angular frequency and k is the wavenumber. For small wavenumbers ($k \ll g\rho/T$), gravity is the dominant force driving the wave motion and the wave is referred to as a gravity wave, the wave speed being inversely proportional to $k^{1/2}$. For large wavenumbers ($k \gg g\rho/T$), surface tension is the dominant driving force and the wave is referred to as a capillary wave, the wave speed being proportional to $k^{1/2}$. In linear wave theory there is no interaction between waves with different wave numbers and in general waves with different wave numbers will travel at different speeds. It is possible, however, for two waves with different wavenumbers to travel at the same speed. This can only occur if one wave is a gravity wave and the other is a capillary wave. When steep waves are considered, linear wave theory is no longer applicable However, the same situation arises where a gravity wave and a capillary wave can travel at the same speed. The situation is complicated because each wave consists of components over a range of wavenumbers, being transfered between these wavenumbers for each wave and between the wavenumbers for both wave types. Energy loss due

to dissipation is greater for the capillary waves and energy cascades from the smaller wavenumbers to the larger wavenumbers in a manner analogous to the energy cascade observed in turbulent fluids. This means that the capillary waves are sustained by energy obtained from the longer gravity waves on which they ride; thus they are referred to as parasitic capillary waves.

An understanding of wave behaviour under a surface slick is important when considering the dispersion of the slick by wave breaking. It may also prove useful for detecting surface films using Synthetic Aperture Radar (SAR). SAR detects radar waves Bragg-scattered by the sea surface and enables ocean wave spectra to be obtained [10]. If variations in the wave spectra observed from SAR images were seen to exhibit the same features as predicted due to the presence of a surface film, then these variations could be used do identify regions of possible contamination. This could prove useful for identifying small scale pollution which might otherwise be difficult to detect but which may, on a large time scale, represent a significant discharge.

6.2 Previous Studies

Parasitic capillary waves have been studied by a number of authors. Experimental investigations have been carried out by Cox [11], Chang *et al.* [12], Ebuchi *et al.* [13], Miller *et al.* [14], Perlin *et al.* [15], Zhang and Cox [16], Zhang [17] and Fedorov *et al.* [18]. These investigations are mainly concerned with determining the surface profile. The amplitude of the capillary waves is typically about 1 mm so an accurate, non-intrusive measuring technique is required. Typically an optical technique which measures the gradient of the surface is used. Analytic and numerical studies of parasitic capillary waves have also been reported by many authors including Longuet-Higgins [19, 20], Crapper [21], Chen and Saffman [22, 23] and Ruvinsky *et al.* [24].

A recent study has been performed by Fedorov and Melville [25]. They consider steady-state gravity-capillary waves which are driven by a forcing term with the length scale of the gravity wave. Energy is removed from the wave system through viscous dissipation. They model an irrotational fluid as their first approximation and treat the viscous nature of the boundary layer as a perturbation. They find surface profiles for parasitic capillary waves on the gravity waves and identify different cases depending on the form of the forcing. Using this approach they combine the Bernoulli equation for a steady viscous flow with the dynamic boundary conditions for a (clean) surface to obtain the Bernoulli equation at the surface which is written

$$\frac{U^2}{2} + gY + \frac{T}{R} + \frac{P_0}{\rho} + \frac{\nu k}{c}\frac{\partial}{\partial \zeta}U^2 = E, \tag{4}$$

where U is the velocity at the surface, g is the acceleration due to gravity, Y is the vertical surface displacement, c is the wave speed, R is the radius of curvature of the wave, P_0 is the forcing term, ρ is the water density, ν is the kinematic viscosity, E is the energy and ζ is used to parameterise the surface. Expressions for the terms in equation (4) are found in terms of the unknowns c, E and a series of Fourier coefficients. The unknowns are then found using an optimisation technique to give a solution for the surface displacement Y. This approach gives a steady state solution for the capillary-gravity waves. By altering the boundary conditions to allow for a surface film and hence arriving at a modified Bernoulli equation, this approach could prove useful in determining the influence of the surface film on the surface displacement and hence on wave breaking.

7 Further Work and Conclusions

Work on the dispersion of surface films and the damping of parasitic capillary waves is continuing. The repeatability of the dispersion under identical breakers, and the effect of multiple breakers and film thickness on dispersion have also been studied; the results will be published later. The same experimental method could be used to investigate other influences such as bed slope and wind.

Dual-plane PIV [26] will be used to measure the velocities present in the water. With this data, it will be possible to compare the motion of the water to the motion of the film. The transition from 2d to 3d motion can be quantified, and the vector maps produced can be used to calculate turbulence statistics [27]. The next stage of this research will thus be to relate the dispersion of the film to the motion of the water.

The effect of a surface film on parasitic capillary waves will be investigated following the approach of Fedorov and Melville [25]. This will involve examining the rate of energy exchange from small to large wavenumbers which occurs in the absence of a surface film and observing how this is altered when a surface film is present.

In conclusion, the technique of LIF has been used to obtain concentration maps of the dispersion of a surface film after breaking. The effect of wave height prior to breaking on this dispersion has been investigated. The fractal dimension of the film's outline, average angle of descent of the centroid and maximum diffusion coefficient all increase with wave amplitude. A technique for studying parasitic capillary waves in the presence of a surface film has been outlined.

8 Acknowledgements

The authors gratefully acknowledge financial support from the Engineering and Physical Sciences Research Council, UK.

References

[1] J. Pullen, A. Arnott, J. M. Buick and C. Greated. Particle image velocimetry study of the effects of surface active films on capillary-gravity waves. To be published in proceedings of EuroMech 387 "Surface slicks and remote sensing of air sea interactions", Warwick UK, 6-8 April 1998.

[2] J. Pullen, A. Arnott, J. M. Buick and C. Greated. Lagrangian motions near the surface of capillary-gravity waves with surface films. To be published in proceedings of EuroMech387 "Surface slicks and remote sensing of air sea interactions", Warwick UK, 6-8 April 1998.

[3] J. S. Fox. *Transport Dynamics of Marangoni Films*. PhD thesis, University of Birmingham, 1996.

[4] J. C. Scott. The propagation of capillary-gravity waves on a clean water surface. *Journal of Fluid Mechanics*, 108:127–131, 1981.

[5] H. Lamb. *Hydrodynamics*. Cambridge University Press, 1962.

[6] J. C. Scott. Oil slicks still the waves. *Nature*, 340:601–602, 1989.

[7] R. J. Rapp and W. K. Melville. Laboratory measurements of deep-water breaking waves. *Philosophical Transactions of the Royal Society of London*, 331:735–800, 1990.

[8] U. Lemmin, J. T. Scott, and U. H. Czapski. The development from two-dimensional to three-dimensional turbulence generated by breaking wave. *Journal Of Geophysical Research*, 79:3442–3448, 1974.

[9] J. Lighthill. *Waves in Fluids*. Cambridge University Press, 1978.

[10] K. Hasselmann and S. Hasselmann. On the nonlinear mapping of an ocean wave spectrum into a synthetic aperture radar image spectrum and its inversion. *Journal of Geophysical Research*, 96:10713–10729, 1991.

[11] C. S. Cox. Measurements of slopes of high-frequency wind waves. *Journal of Marine Research*, 16:199–225, 1958.

[12] J. H. Chang, R. N. Wagner, and H. C. Yuen. Measurement of high frequency capillary waves on steep gravity waves. *Journal of Fluid Mechanics*, 86:401–413, 1978.

[13] N. Ebuchi, H. Kawamura, and Y. Toba. Fine structure of laboratory wind-wave surfaces studied using an optical method. *Boundary-Layer Meteorology*, 39:133–151, 1987.

[14] S. Millar, O. Shemdin, and M. Longuet-Higgins. Laboratory measurements of modulation of short wave slopes by long surface waves. *Journal of Fluid Mechanics*, 233:389–404, 1992.

[15] M. Perlin, H. Lin, and C.-L. Ting. On parasitic capillary waves generated by steep gravity waves: An experimental investigation with spatial and temporal measurements. *Journal of Fluid Mechanics*, 255:597–620, 1993.

[16] X. Zhang and C. S. Cox. Measuring the two dimensional structure of a wavy water wave surface optically: A surface gradient detector. *Experiments in Fluids*, 17:225–237, 1994.

[17] X. Zhang. Capillary-gravity and capillary waves generated in a wind tank: Observations and theories. *Journal of Fluid Mechanics*, 289:51–82, 1995.

[18] A. V. Fedorov, W. K. Melville, and A. Rozenberg. An experimental and numerical study of parasitic capillary waves. *Physics of Fluids*, 10:1315–1323, 1998.

[19] M. S. Longuet-Higgins. The generation of capillary waves by steep gravity waves. *Journal of Fluid Mechanics*, 16:138–159, 1963.

[20] M. S. Longuet-Higgins. Parasitic capillary waves: A direct calculation. *Journal of Fluid Mechanics*, 301:79–107, 1995.

[21] G. D. Crapper. Non-linear capillary waves generated by steep gravity waves. *Journal of Fluid Mechanics*, 40:149–159, 1970.

[22] B. Chen and P. G. Saffman. Steady gravity-capillary waves on deep water - II. Weakly nonlinear waves. *Studies in Applied Mathematics*, 60:183–210, 1979.

[23] B. Chen and P. G. Saffman. Steady gravity-capillary waves on deep water - II. Numerical results for finite amplitude. *Studies in Applied Mathematics*, 62:95–111, 1980.

[24] K. D. Ruvinsky, F. I. Feldstein, and G. I. Freidman. Numerical simulation of the quasi-stationary stage of ripple excitation by steep gravity-capillary waves. *Journal of Fluid Mechanics*, 230:339–353, 1991.

[25] A. V. Fedorov and W. K. Melville. Nonlinear gravity-capillary waves with forcing and dissipation. *Journal of Fluid Mechanics*, 354:1–42, 1998.

[26] M. Raffel, J. Westerweel, C. Willert, M. Gharib, and J. Kompenhans. Analytical and experimental investigations of dual-plane particle image velocimetry. *Optical Engineering*, 35:2067–2074, 1996.

[27] T. R. Haydon. *Turbulence and Vorticity Generated by Breaking Waves*. PhD thesis, The University of Edinburgh, 1997.